A&A 366, 146–156 (2001)
DOI: 10.1051/0004-6361:20000095

Astronomy & Astrophysics

On the history of the interplay between HD 56925 and NGC 2359

J. R. Rizzo[1,⋆], J. Martín-Pintado[1], and J. G. Mangum[2]

[1] Observatorio Astronómico Nacional, Aptdo. Correos 1143, 28800 Alcalá de Henares, Spain
[2] NRAO, 949 N. Cherry Avenue, Tucson, AZ 85721, USA

Received 20 October 2000 / Accepted 03 November 2000

Abstract. NGC 2359 is an optical nebula excited by the powerful wind and the radiation of the Wolf–Rayet star HD 56925. We have investigated the interaction between this massive star and the surrounding neutral gas by analyzing the large-scale 21 cm-HI emission and by mapping the nebula in the $J = 1 \rightarrow 0$ and the $J = 2 \rightarrow 1$ lines of CO. We found a conspicuous (70×37 pc) HI shell, expanding at 12 km s^{-1}, likely produced during the main-sequence phase of the star. The molecular gas towards NGC 2359 shows three velocity components. Two of these components, A1 and A2, have narrow linewidths (1–2 km s^{-1}) and radial velocities of 35–38 and 64–68 km s^{-1}, respectively. The third component is detected at radial velocities between 50 and 58 km s^{-1} and has a broader profile (up to 5.5 km s^{-1}). Furthermore, this component is morphologicaly related with the nebula and has a velocity gradient of a few km s^{-1}. We have also estimated the physical parameters of the molecular gas by means of a LVG modelling of the CO emission. The gas projected onto the southern HII region of the nebula has low CO column density and is rather hot, probably up to 80 K. Several profiles of the ^{13}CO $J = 1 \rightarrow 0$ line near the peak of the emission, together with a weak emission bridge between the broad and one of the narrow components (component A2), suggest the presence of a shock front acting in the southern part of the nebula. This shock was likely produced in a previous RSG/LBV phase of HD 56925.

Key words. stars: individual (HD 56925) – stars: Wolf–Rayet – stars: winds – ISM: bubbles – ISM: individual (NGC 2359) – ISM: kinematics and dynamics

1. Introduction

The different evolutive stages of massive stars have strong influence on their surroundings and, consequently, on the galactic evolution. During their lives, the massive stars inject large amounts of matter, energy and momentum into the interstellar medium (ISM). In the pre-main sequence, massive stars undergo a phase of very energetic mass loss giving rise to molecular outflows. UV radiation, expansion of HII regions and fast stellar winds are present in the main sequence stage. In the short–lived red supergiant (RSG) and luminous blue variable (LBV) stages, the winds become slower and denser and ejections of up to some solar masses may be produced. The Wolf–Rayet (WR) stage, prior to SN explosions, is characterized by a copious mass loss (typically 10^{-5} $M_\odot$ yr^{-1}) driven by a fast (about 2000 km s^{-1}) and chemically enriched stellar wind. Massive stars are therefore continuously heating, ionizing, shocking and blowing-up the ISM surrounding them. García-Segura & Mac Low (1995) have modeled the evolution of the gas which surrounds massive stars, from the main sequence to the WR stage. They only considered simple models for the mass ejection in the form of stellar winds in the different stages of evolution and predict the presence of large scale structures around the massive stars. Both the blown-up gas and the ejecta form multiple shells as a consequence of the different shockfronts produced inside the gas.

During the main sequence phase, the gas around massive stars is ionized, heated and highly evacuated by the fast, long-lived stellar wind and the Lyman continuum radiation. A hot cavity is surrounded by an expanding shell. The ionization front may get trapped within it, the shell may start to recombine and become observable in the line radiation emitted by neutral atoms or molecules. These large bubbles have been successfully detected in the 21-cm line of atomic hydrogen (Arnal 1992; Rizzo & Bajaja 1994; Cappa & Benaglia 1998; Rizzo & Arnal 1998; Arnal et al. 1999), in the form of huge shells of 30–70 pc, expanding at 6–20 km s^{-1}, with masses of hundreds (or even thousands) of solar masses. Some of the large IRAS shells found by Marston (1996) might also be related to this type of structures.

Send offprint requests to: J. R. Rizzo
⋆ On leave of absence from Instituto Argentino de Radioastronomía, Argentina.

Once the massive star finishes the hydrogen burning in its nucleus and becomes a RSG or LBV, its stellar wind suddenly becomes more dense, and a significant amount of the stellar mass is deposited into the ISM at velocities around 20 km s^{-1}. Very probably, the formation of the optical ring nebulae starts in this brief stage. When the star comes to a WR stage, the wind is accelerated to hypersonic velocities and rapidly reaches the RSG/LBV wind. Many of the optical nebulae possess arcs and have high inhomogeneities in the abundances of heavy elements (Chu et al. 1983, 1999).

However, the effects of the WR phase in the neutral (neither atomic nor molecular) gas have not been easily detected. The structures formed during this phase would not be as large as those developed in the O-phase. Just in few cases, the neutral atomic hydrogen has been detected in interaction with ring nebulae (Cappa et al. 1996; Arnal & Cappa 1996). Vibrationally excited molecular hydrogen has only been detected towards NGC 2359. The CO $J = 1 \rightarrow 0$ emission has been observed around WR 16 (Marston et al. 1999) and in NGC 2359 (Schneps et al. 1981).

NGC 2359 is a very interesting object, and many aspects of which has been thoroughly studied in the recent years. This optical nebula is excited by HD 56925 (WR 7 in the catalogue of van der Hucht (2000), a WN4 star located in the outer Milky Way. Its distance varies from 3.5 to 6.9 kpc depending on the authors (see Goudis et al. 1994 for a discussion). The mass–loss rate ($< 7\ 10^{-5}\ M_{\odot}$ yr^{-1}) and the terminal wind velocity (1545 km s^{-1}) have been measured by Schneps et al. (1981) and Rochowicz & Niedzielski (1995), respectively. NGC 2359, a prototypical wind-blown bubble (Chu et al. 1983), is nearly spherical with several small filaments inside. The nebula is not highly enriched of heavy elements as a whole, with the exception of the filaments (Esteban et al. 1990). This may indicate that the nebula was largely produced in the RSG/LBV and the WR stages of the exciting star. From the optical emission lines (Goudis et al. 1983) and radio recombination lines (Lockman 1989; Fich & Silkey 1991), we know that the ionized gas has several components at velocities between 30 and 70 km s^{-1} (all velocities in this paper are referred to LSR). An HII region partially surrounds the wind-blown bubble and is apparently limited by obscuring material. Schneps et al. (1981) have taken several profiles in the $J = 1 \rightarrow 0$ line of CO and detected the presence of three clouds at 37, 54 and 67 km s^{-1}. The presence of broad CO profiles at 54 km s^{-1} and the morphology of the emission, just following the south-eastern edge of the nebula, suggests that this component has been interacting with the nebula. St-Louis et al. (1998) have analyzed the H_2 emission in this region. They have found the 1–0 $S(1)$ line towards the southern border of the HII region, but they could not establish the nature of the excitation (fluorescence or shocks) of the H_2. Cappa et al. (Cappa et al. 1999) made a complete map of the ionized component at the 1465 MHz continuum, and traced the HI emission presumably connected with the nebula. These HI features are probably associated with the WR stage of HD 56925; so far, the large atomic main-sequence bubble predicted by the theory has not been yet reported.

The goal of this paper is to look into the history of the interaction of the wind and the radiation of HD 56925 and its surroundings. We have analyzed a public HI survey and studied for the first time the large scale interaction of HD 56925 in the O-phase with the ambient ISM. Based on the mapping of the $J = 1 \rightarrow 0$ and $J = 2 \rightarrow 1$ lines of CO over the whole optical nebula, we study in detail the morphology and kinematics of the CO around NGC 2359. We also present several ^{13}CO profiles towards selected positions in order to determine the global physical parameters of the molecular gas, such as kinetic temperature, density and opacity of the lines. This study has allowed us to shed some light on the dominant excitation mechanism of the neutral gas in the WR stage.

2. Observational material

2.1. The HI survey

We have analyzed a region of $6^{\circ} \times 6^{\circ}$ around NGC 2359 using the 21 cm–HI survey of Hartmann & Burton (1997). This survey was made using the 25 m radio telescope at Dwingeloo. The angular and velocity resolution of this dataset are $36'$ and 1.03 km s^{-1}, respectively. The survey has been done with a sampling of $30'$ in galactic coordinates and have a sensitivity in brigthness temperature of 70 mK.

2.2. CO observations

The observations of the CO $J = 1 \rightarrow 0$ (115.271 GHz) and $J = 2 \rightarrow 1$ (230.538 GHz) lines and the $J = 1 \rightarrow 0$ (110.201 GHz) line of ^{13}CO towards NGC 2359 and its surroundings were made during 2000 February, using the NRAO[1] 12 m radio telescope at Kitt Peak. The half power beam width of the telescope was $54''$ and $27''$ at the rest frequency of the $J = 1 \rightarrow 0$ and the $J = 2 \rightarrow 1$ lines, respectively.

The data were acquired simultaneously with two independent SIS receiver channels with orthogonal polarizations. The receiver temperatures were 250–300 K and 500–600 K for the $J = 1 \rightarrow 0$ and the $J = 2 \rightarrow 1$ lines, respectively. We used filterbanks (with 256 channels) and the hybrid correlator MAC (in the 2 IF mode, in parallel, 3072 channels) as backends. In the $J = 1 \rightarrow 0$ line, the filterbanks provided 100 and 250 kHz of resolution, corresponding to velocity resolutions of 0.26 and 0.65 km s^{-1}, respectively. For the same line, the MAC correlator was setup with a total usable bandwidth of 300 MHz and with channels of 195.3 kHz of resolution (0.51 km s^{-1}). In the $J = 2 \rightarrow 1$ line, the filterbank with channel widths of

[1] The National Radio Astronomy Observatory is operated by Associated Universities, Inc. under cooperative agreement with the National Science Foundation.

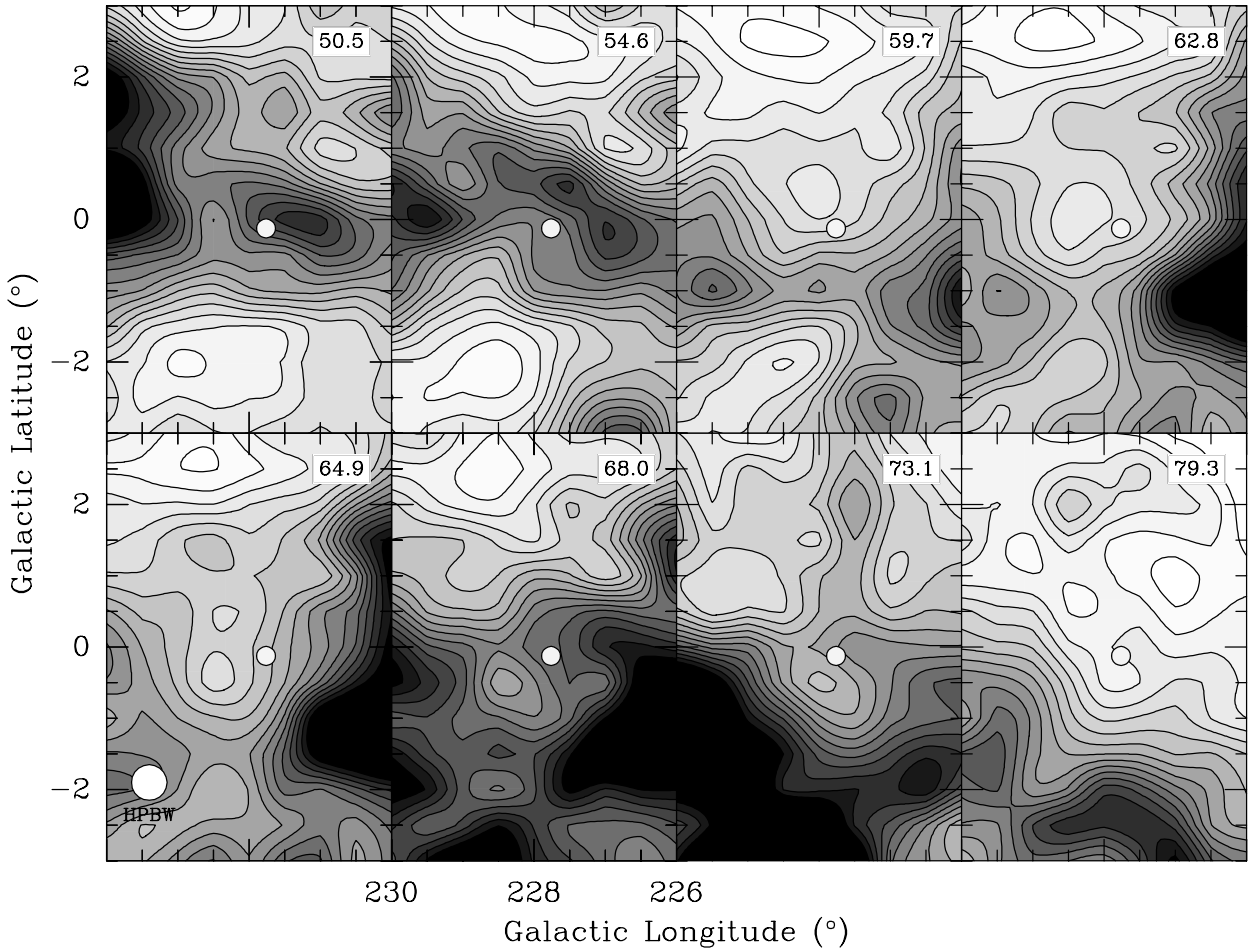

Fig. 1. Distribution of the 21 cm–HI column density in a large region around NGC 2359, obtained from the survey of Dwingeloo (Hartmann & Burton 1997). Every map has been constructed integrating over 2.1 km s^{-1} (2 channels), being the central velocity of integration indicated at the top right corner. Contour levels are 3 to 18 times 10^{19} cm^{-2}. The small circle near the centre indicates the position and size of NGC 2359. The Dwingeloo beam is also plotted in the bottom left map

250 kHz (0.33 km s^{-1}) and 500 kHz (0.65 km s^{-1}) were used. We also used for this line the MAC correlator tuned with an usable bandwidth of 600 MHz and frequency resolution of 390.6 kHz (0.51 km s^{-1}).

Mapping of the $J = 1 \rightarrow 0$ and $J = 2 \rightarrow 1$ lines was made using the "on-the-fly" technique. We have obtained three individual maps in the $J = 1 \rightarrow 0$ line and six in the $2 \rightarrow 1$ line. These individual maps were later reduced with AIPS and combined weighting them by their inverse square of rms. For our investigation, we finally used the MAC data for the $J = 1 \rightarrow 0$ line and the 500 kHz-filterbank data for the $J = 2 \rightarrow 1$ line. Typical final rms per grid point was 120 mK and 80 mK in the $J = 1 \rightarrow 0$ and $J = 2 \rightarrow 1$ lines, respectively. We have also observed the $J = 1 \rightarrow 0$ line of ^{13}CO and C^{18}O at seven individual positions, with 7–10 min of integration time achieving a rms noise of 30 mK.

The pointing was checked at the begining of each observing session with five–point cross maps. The final data are pointed within 4″ of uncertainty. The data were calibrated using the chopper wheel method. Final intensity scale is in units of $T_{\rm R}^{*}$, e.g., corrected by atmospheric attenuation and instrumental losses (Kutner & Ulich 1981). The calibration was also checked off-line by comparing individual spectra of standard sources.

3. Results

3.1. Neutral hydrogen

We have analyzed the HI data in the velocity range 20–80 km s^{-1}, e.g., the velocity range of the optical and the CO emission. According to most of the galactic rotation models (for example Fich et al. 1989), this broad range in velocity is expected for the range of distances associated to HD 56925 (Goudis et al. 1994). Within this velocity range, we looked for the structures connected to the evolution of HD 56925.

Figure 1 depicts HI column density ($N_{\rm HI}$) maps as a function of the radial velocity, indicated at the top left corner. The white circle near the center of the map sketchs the position and size of NGC 2359. Every map shown in Fig. 1 has been obtained by the integration of the

Table 1. Main parameters of the HI bubble

Parameter	Unit	Value
Systemic velocity	km s^{-1}	64
Velocity range	km s^{-1}	51 to 76
Major axis[a]	pc	70
Minor axis[a]	pc	37
HI mass, lower limit[a]	$M_\odot$	700
HI mass, upper limit[a]	$M_\odot$	2400

[a] For an assumed distance of 5 kpc.

brightness temperature over 2.1 km s^{-1} (2 channels) and assuming optically thin emission.

We have found an outstanding structure which remains coherent across tens of velocity channels. This structure is a huge cavity surrounded by a set of relative maxima in the $N_{\rm HI}$ maps. The centroid of this cavity remains approximately at the same point, and nearly off-centered from the nebula and the WR star. The excentric position of the WR star with respect to the cavity is also observed in almost all the WR bubbles (Arnal 1992) and might be due to the star motions and/or density variations in the original ISM (Moffat et al. 1998). The structure reaches its maximum size at velocities between 61 and 65 km s^{-1}. For receding and approaching velocities with respect to this velocity interval, the cavity diminishes its angular size, ending at ∼51 and 76 km s^{-1} with small relative maxima centered at the cavity.

The morphology of this structure has the typical ring–disk appearence of an expanding bubble. Following the standard analysis of this type of shells, the largest size of the cavity indicates the geometrical dimensions and its radial velocity corresponds to approximately the systemic velocity of the gas before the expansion. The full velocity range where the feature is observed gives a lower limit of twice the expansion velocity. Table 1 summarizes the parameters derived, as described above, for the expanding cavity. Following Arnal et al. (1999), we have also derived lower and upper limits to the mass of the HI shell. These two values for the HI mass are the missing mass into the higher close contour and the neccesary mass to fill the cavity making it indistinguishable of the nearly environs. All distance-dependent parameters were calculated assuming a distance of 5 kpc.

This HI shell is in geometrical coincidence with the IRAS shell reported by Marston (1996). Furthermore, the mass of gas predicted from the IRAS data falls within the HI estimates presented in Table 1.

3.2. Carbon monoxide

3.2.1. Morphology and kinematics

The CO emission in the $J = 1 \rightarrow 0$ and $J = 2 \rightarrow 1$ lines are observed in three velocity components. The components with the lowest radial velocity (35–38 km s^{-1}) and with the highest radial velocity (64–69 km s^{-1}) show narrow profiles of 1.5–2.5 km s^{-1} width. Hereafter we will refer to these two components as Ambient 1 (A1) and Ambient 2 (A2), respectively. The third component, with radial velocities of 50–58 km s^{-1}, shows broader profiles than the components A1 and A2, having linewidths of 4–5.5 km s^{-1}. We will refer to this component as Broad component (B). Figure 2 shows the global spatial distribution of the CO $J = 1 \rightarrow 0$ (left panels) and $J = 2 \rightarrow 1$ (right panels) integrated emission for the three components. For comparison, the CO maps have been overlaid with a J band image of NGC 2359, obtained from the *Digitized Sky Survey*. At the top right corner of each panel, the velocity interval of integration is indicated. The mapped regions in both spectral lines are also depicted. In the $J = 1 \rightarrow 0$ line, almost all the optical nebula and its surroundings has been covered by our observations. In the $J = 2 \rightarrow 1$ line, however, we limited the maps at the east and the north-west because of our interest in studying in detail the interaction of the nebula with the molecular gas.

The CO emission for components A1 and A2 appear mainly to the east and to the south-east of the mapped regions, respectively. Although the spatial distribution for both components are found close in projection to the optical nebula, there is not a clear morphological correlation. Furthermore, there are no significant changes in the line widths and in the peak velocities over the regions where these components are observed. In contrast, the broad component B is observed in clear correlation with the eastern and the southern edges of NGC 2359, and with broader profiles, varying from 4 to 5.5 km s^{-1} wide.

The most intense CO emission of component B is located beyond the outer edge of the HII region in NGC 2359, mainly to the south-east part, but also significant emission in the $J = 2 \rightarrow 1$ line is detected towards locations projected on the HII region (middle right panel in Fig. 2). For a comparison between the spatial distribution of the $J = 1 \rightarrow 0$ and $2 \rightarrow 1$ lines of CO for the component B, the Fig. 3 shows and overlay of the emission in the $J = 1 \rightarrow 0$ line (solid lines) and the $J = 2 \rightarrow 1$ line (dashed lines) convolved to the resolution of the $J = 1 \rightarrow 0$ line. This comparison shows that both lines are well correlated at the most intense and the external part of the nebula. However, we note again that the $J = 2 \rightarrow 1$ line have significant extended emission to the inner part of NGC 2359, especially into the southern optical filament. This is clearly ilustrated in the left and right panels in Fig. 3, where we show a sample of four CO $J = 1 \rightarrow 0$ and $2 \rightarrow 1$ line profiles toward the positions sketched by squares in the central map. The lower left spectra show the mean profiles around the most intense region, while the other three panel show the CO profiles in the periphery of the CO emission. There is a clear trend in the profiles. While the $J = 1 \rightarrow 0$ line is stronger than the $J = 2 \rightarrow 1$ line toward the most intense zone of emission, the $J = 1 \rightarrow 0$ line is much weaker than the $J = 2 \rightarrow 1$ line or it is not detected in positions closer to the HII region. The $2 \rightarrow 1/1 \rightarrow 0$ intensity ratio varies from 0.8–1 near the

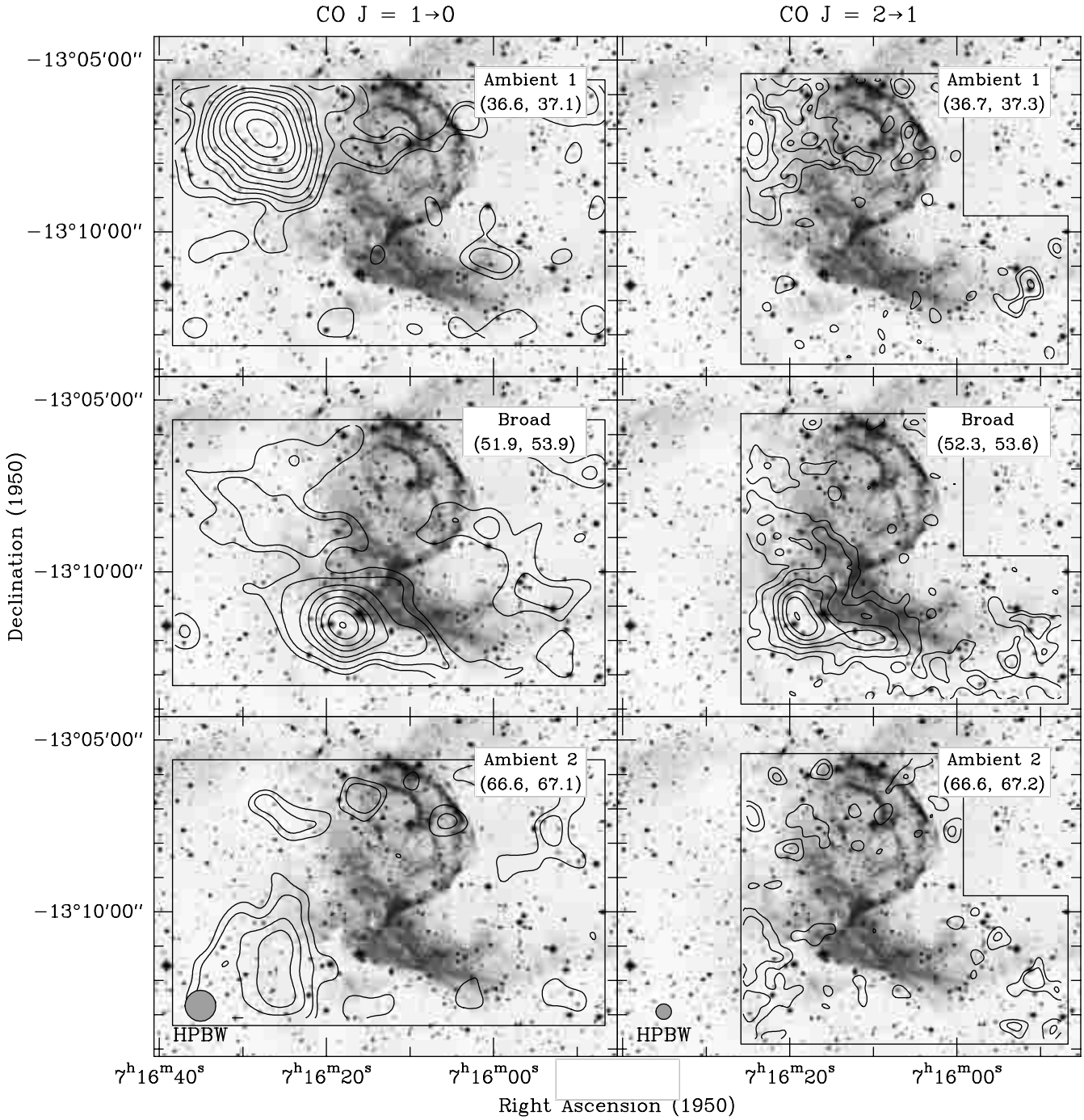

Fig. 2. CO emission in the field of NGC 2359. The three maps at left correspond to the $J = 1 \rightarrow 0$ line, while the three maps at right correspond to the $J = 2 \rightarrow 1$ line. The three principal components detected are named as Ambient 1 (A1), Broad (B) and Ambient 2 (A2), indicated at the top right corner of every map, together with the velocity of integration in km s^{-1}. Beams are also depicted at the bottom maps. The polygons drawn enclose the mapped regions in both spectral lines. Contour levels are (1, 2, 4, 6, 9, 12, 16, 20, 25 and 30) times 0.2 K km s^{-1} (components A1 and A2, $J = 1 \rightarrow 0$ line), 0.3 K km s^{-1} (A1 and A2, $J = 2 \rightarrow 1$ line) or 0.5 K km s^{-1} (component B, both lines). The optical image of NGC 2359 has been obtained from the *Digitized Sky Survey*

peak to 1.5–2 towards the positions near the HII region. In contrast, the $2 \rightarrow 1/1 \rightarrow 0$ intensity ratio is nearly constant in components A1 and A2, with values around 0.5–0.6.

While the components A1 and A2 do not have any remarkable kinematical features, the component B have slightly different peak velocities as a function of the position. Figure 4 shows four position-velocity diagrams, taken in the directions sketched in the map of the $J = 2 \rightarrow 1$ emission at the top left corner of this figure. Each position-velocity diagram is identified by the slice number. Slice 1 shows the most intense part of component B at

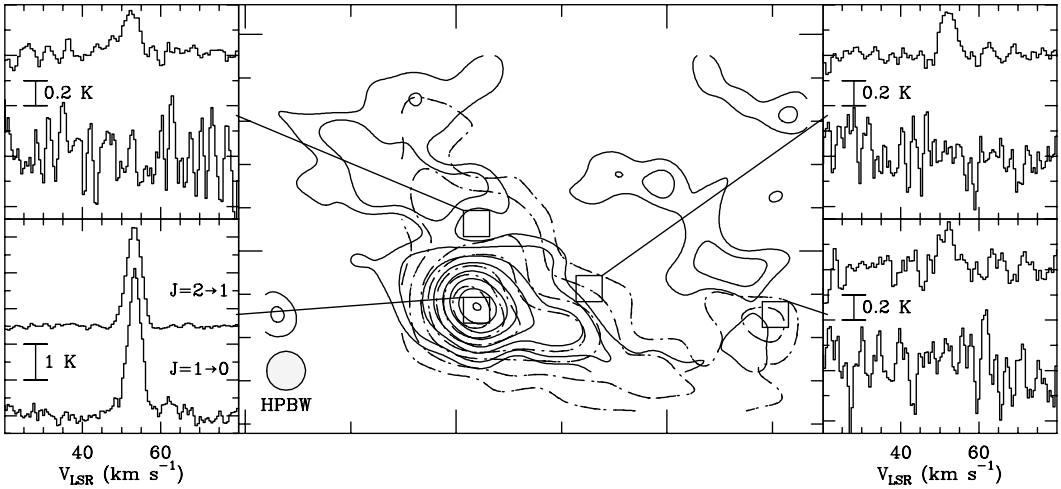

Fig. 3. Comparison of the emission between the two observed transitions of CO in the B component. In the central panel, solid lines represent the $J = 1 \rightarrow 0$ intensity, while the dashed ones represent the $J = 2 \rightarrow 1$ intensity, convolved to the $J = 1 \rightarrow 0$ resolution. Contour levels are (1, 2, 4, 6, 9, 12 and 16) times 0.5 K km s^{-1}. Four selected positions are indicated by squares, and their spectra plotted at left and right panels. Every panel displays the $J = 2 \rightarrow 1$ spectrum above the $J = 1 \rightarrow 0$ spectrum

53–54 km s^{-1} and the western border of the component A2. Slice 1 also shows hints of a small velocity gradient in the component B. This is more clearly depicted in the slice 2, where we find along the central part a velocity shift of $\sim$2 km s^{-1}. Both slices 1 and 2 remarks the spatial coincidence between the eastern border of component B and the western border of component A2. In fact, slice 3 shows the presence of a weak (4 σ) "bridge" in the CO emission which connects the components B and A2. This suggests a physical connection between both components. Slice 3, parallel to the slice 2 but 1′ to the south-west, does not show signs of this "bridge", indicating the small size and weakness of this bridge. The slice 4 show that the diffuse emission to the north have a radial velocity slightly lower than that of the main part of the component B.

3.2.2. ^{13}CO $J = 1 \rightarrow 0$ emission in component B

In order to study the excitation of the CO line in the component B, we have observed seven positions in the ^{13}CO and C^{18}O $J = 1 \rightarrow 0$ lines, towards the southern part of NGC 2359. The location of the observed points are shown in Fig. 5a, superimposed on a CO $J = 2 \rightarrow 1$ map of the component B. Five of these positions are located close to the slice 1. Figures 5b, 5c and 5d plot three of these ^{13}CO $J = 1 \rightarrow 0$ profiles (labeled with letters b, c and d in the circles of Fig. 5a), together with the ^{12}CO $J = 1 \rightarrow 0$ spectra of the same points. We find a significant variation in the ^{12}CO/^{13}CO ratio. This ratio is $\sim$6 for the CO emission peak (Fig. 5b) and increases to values >30 elsewhere.

Another interesting result is that the ^{12}CO/^{13}CO ratio does not only vary with position but also it changes with radial velocity within the beam towards the CO emission peak (Fig. 5b). One can see that both lines peak at different velocities. The ^{13}CO line appears shifted by $\sim$1–2 km s^{-1} with respect to that of ^{12}CO. This shift produces important changes in the ^{12}CO/^{13}CO ratio as a function of the radial velocity. The ^{12}CO/^{13}CO ratio is $\gtrsim$30 at 50–53 km s^{-1}, and decreases to $\sim$4–5 for radial velocities between 54 and 57 km s^{-1}. In view of the small velocity gradient found in the component B, we do not think that this shift can be due to a pointing error between the ^{12}CO and ^{13}CO data. Even in the worst possible case, 10″ of pointing difference, we find that this ratio would change with radial velocity by at least a factor of 4 for velocities below and above 53 km s^{-1}.

4. Discussion

4.1. Origin of the HI expanding shell

The HI structure found in this paper resembles the expanding shells often associated with O stars (Cappa & Benaglia 1998), WR stars (Arnal 1992; Arnal et al. 1999) and OB associations (Rizzo & Bajaja 1994; Rizzo & Arnal 1998). In the following we shall explore if the HI shell has been created by the stellar wind from HD 56925 or from its O–progenitor. Let us estimate, with a few assumptions, some important parameters to distinguish between the two possibilities. We shall consider a spherical expanding bubble, with a radius of 50 pc, an expansion velocity of 12 km s^{-1}, and a mass of 1500 $M_{\odot}$. With these values, we estimate a dynamical time for the shell of 2.3 Myr and a kinetic energy of 2.2 10^{48} erg. The dynamical time was computed as a mean value between the adiabatic and the radiative case (McCray 1983). This time is in fact an upper limit, but a good approximation, to the age of the HI structure (Dyson 1989). This age and the kinetic energy associated to the HI shell clearly indicate that its origin is due to the main-sequence phase of HD 56925. Indeed, the most massive stars, greater than 25 $M_{\odot}$, remains a few million years at the main sequence (Maeder & Meynet 1994) and creates

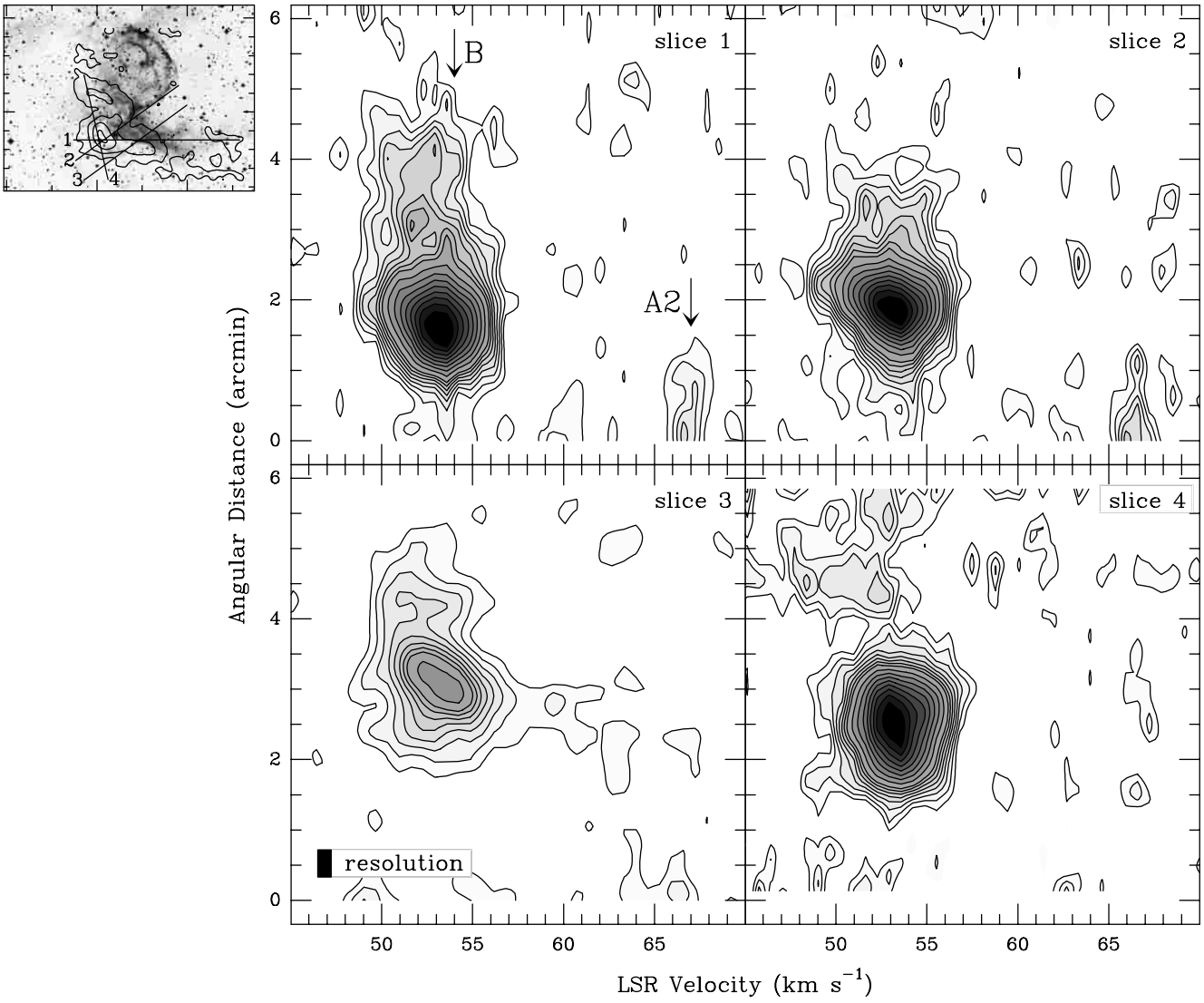

Fig. 4. Four strips in position for the $J = 2 \rightarrow 1$ emission of CO. The location of the slices are sketched by right lines in the small map at the top left of the figure. The numbers indicate the slice number and the origin of the angular distance scale in the four slices. Contour levels are 1 to 8 times 0.2 K and 5 to 12 times 0.4 K. Resolution in both position and velocity are plotted in slice 3. Arrows indicate the location of the components A2 and B

interstellar bubbles of 30–60 pc in this stage (Weaver et al. 1977; García-Segura & Mac Low 1995). It is thought that WR's are descendant of these massive stars. On the other hand, the RSG, LBV or WR phases are short-lived, probably 10^4–10^5 yr (Maeder & Meynet 1994; Langer et al. 1994). We therefore conclude that only the O progenitor of HD 56925 had sufficient time to develop the HI expanding shell reported in this paper. A similar conclusion was reached by Marston (1996) concerning to the large IRAS shell found around several WR stars, including the one linked to HD 56925.

By adopting typical values for the mass-loss rate of 10^{-6} $M_\odot$ yr^{-1} and a wind velocity of 1000 km s^{-1} for the O–progenitor star, we estimate that this star deposited into the ISM during 2.3 Myr a total energy of $\sim$2.3 10^{49} erg in the form of stellar wind. If this star has blown up the shell which we are observed in HI, it implies a kinematical efficiency of nearly 10%. Although the uncertainties in these computations are large and hard to be estimated, this value for the efficiency is in good agreement with the models that predict this type of structures (Weaver et al. 1977; Van Buren 1986) and reinforces our hypothesis of a main sequence origin of the HI shell.

4.2. Physical parameters of the molecular gas

We have estimated the physical parameters of the molecular gas from the CO line emission by modelling the excitation of the CO lines using the *Large Velocity Gradient* (LVG) approximation. For comparison with the model, we have smoothed the $J = 2 \rightarrow 1$ line data to the $J = 1 \rightarrow 0$ resolution. For component B, the ^{13}CO data was also taken into account in order to estimate the opacity of the ^{12}CO lines. Six different components have

Table 2. Physical parameters of the CO emiting regions

Component	$\frac{2\rightarrow1}{1\rightarrow0}$	$\frac{^{12}CO}{^{13}CO}$	T_{ex} K	$n(H_2)$ 10^3 cm^{-3}	$N(CO)$ 10^{16} cm^{-2}	τ_{10}	τ_{21}	$\tau(^{13}CO)$	$m(H_2)$ $M_\odot$
A1	0.5	—	5	0.6	1.0	0.6	0.6	—	96
A2	0.5	—	6	1.0	0.4	0.8	0.8	—	28
B_{all}	0.8	—	8	1.8	0.5	0.3	0.4	—	160
B_{max}^{blue}	1.0	30	10	5.0	1.6	0.6	0.8	< 0.1	10
B_{max}^{red}	1.0	5	10	58	21.	12	—	~ 0.1	120
B_{HII}	2.0	$\gtrsim 30$	$\gtrsim 80$	< 1.6	0.1	<0.1	0.2	≤ 0.1	$\lesssim 8$

The LVG approximation was used in all cases but B_{max}^{red}. For this particular region, we have estimated the size of the emiting region and taken into account the beam filling factor. All masses were computed by assuming a distance of 5 kpc.

been defined. The first three are the ambient components A1 and A2 and the most extended emission of the component B (hereafter B_{all}). The fourth component considered is the one projected onto the southern HII region, named as B_{HII}. Finally, we also considered the region around the CO maxima in component B, where the ^{13}CO behaviour is striking. We have subdivided this component in the two velocity ranges having the greatest difference in the ^{12}CO/^{13}CO ratio (see Fig. 5b), named as B_{max}^{blue} (for the velocity interval 50–54 km s^{-1}) and B_{max}^{red} (for the velocity interval 54–58 km s^{-1}). The results derived from the LVG analysis are shown in Table 2. This table gives estimates for the excitation temperature (T_{ex}), H_2 density ($n(H_2)$), CO column density ($N(CO)$), the opacities of the CO $J = 1 \rightarrow 0$, CO $J = 2 \rightarrow 1$ and ^{13}CO $J = 1 \rightarrow 0$ lines, and the total mass of the regions ($m(H_2)$), derived from the two line ratios (second and third columns) and the ^{13}CO intensities. A kinetic temperature (T_K) of 10 K was assumed for all the regions but B_{HII}. The physical conditions in B_{HII} seem to be very different from those of the other regions. The large ratio between the $J = 2 \rightarrow 1$ and the $J = 1 \rightarrow 0$ lines is explained by optically thin emission with relatively high T_K. The most likely T_K is about 80 K and we present in Table 2 the results derived for this T_K. Components A1 and A2 are subtermally excited ($T_{ex} < T_K$), with typical T_{ex} of 5–6 K. We obtain higher excitation temperatures in component B. For B_{max}^{blue} and B_{max}^{red}, we derived T_{ex} similar to T_K, indicating that the lines are thermalized, and densities significantly higher than for A1 and A2.

For B_{max}^{red} we did not apply the LVG method since this region has a very low value of the ^{12}CO/^{13}CO ratio. Such low value for this ratio usually indicates the presence of a region of very high opactiy in the ^{12}CO lines. Since we have found this low ratio toward only one observed position, we conclude that the emiting region corresponding to B_{max}^{red} is unresolved by the $J = 1 \rightarrow 0$ beam. To derive the physical properties in this component, we have assumed an optically thin emission for the ^{13}CO and optically thick emission of the ^{12}CO. For a ^{12}CO/^{13}CO isotopic ratio of 60 (Wilson & Matteucci 1992), we derive an optical depth of 12 for the $J = 1 \rightarrow 0$ line of ^{12}CO. From the ^{12}CO $J = 1 \rightarrow 0$ line intensity and assuming that the emission in this line is thermalized to the T_K of 10 K, we derive a beam filling factor for B_{max}^{red} between 0.1 and 0.2. With the optical depth we have estimated $N(CO)$. Adopting a beam filling factor of 0.15 and a fractional abundance for CO of 10^{-4} we have also estimated $n(H_2)$. Although our estimates of the H_2 density can be uncertain because of the unknown T_K, the large differences in the H_2 density between B_{max}^{red} and the other components indicate that a rather small region has a density larger than other components.

4.3. Molecular gas interacting with the nebula and the WR star

In Sect. 3.2 we have discussed the morphological and kinematical arguments for the relationship between the different CO components and NGC 2359. In the previous section, we have derived their physical conditions. In this section, we shall consider our observational findings together with those already published, in order to address the nature and the origin of the interaction of the molecular gas with the nebula and its exciting WR star. The component A1 is located mainly to the NE of the map, while the component A2 is present to the SE of the nebula. Both components are narrow (2 km s^{-1}) and do not show any morphological or kinematical structures that indicate any disturbance produced by the nebula or the WR star. In contrast, the component B has some kind of ubiquity in this field, in agreement with optical emission lines like the [O 3]. It appears as a broad component (4.5–5 km s^{-1}) following the east and the south border of the HII region which surrounds the nearly-spherical bubble. We noted that the CO emission is stronger *outside* the optical border of the HII region, but significant emission is also present in projection *onto* the HII region. We think that the component B is the only component which undoubtely interacts with NGC 2359, because of its morphology, the large width of the lines, the higher temperature and the striking kinematics.

As already mentioned, the eastern part and the southern border of the HII region are clearly bounded by the

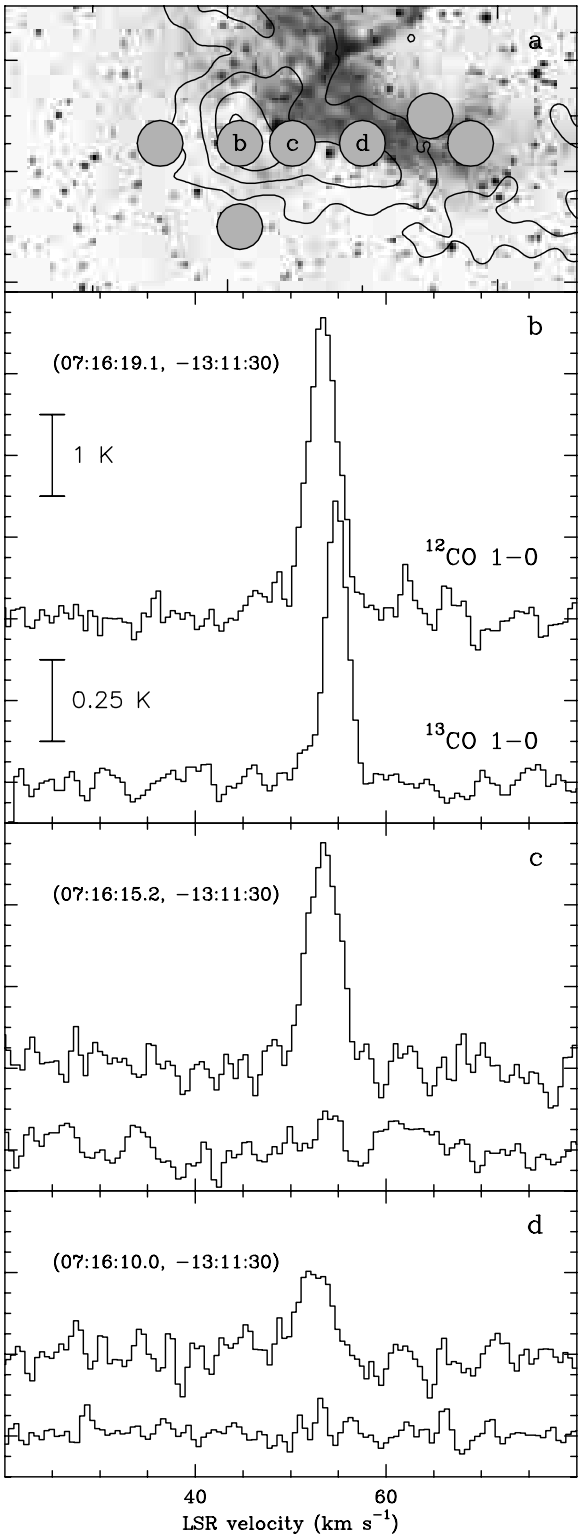

Fig. 5. Comparison of the ^{12}CO and ^{13}CO $1 \rightarrow 0$ lines in three selected positions, indicated at the upper left of every figure. **a)** reproduces part of the $J = 2 \rightarrow 1$ map of component B, superimposed to the positions where the ^{13}CO $J = 1 \rightarrow 0$ line was observed. Letters b, c and d inside three of these circles indicate the position of the profiles shown in panels **b**, **c)** and **d)**, respectively. Different scale was used for both isotopes. We note the remarkable variations in the ^{12}CO/^{13}CO ratio from one point to another, and the different velocity peaks of the isotopes in panel **b)**

most intense component B. Furthermore, the presence of faint CO emission perfectly correlated with the HII region it is also striking. These results are also in agreement with the vibrationally excited H_2 emission observed at 2.2 μm (St-Louis et al. 1998). The CO emission is dense and more opaque outside the HII region, while onto the HII region it is less dense and has a higher temperature (up to 80 K). This temperature is compatible with the dust temperature inferred by Marston (1991) in the same region.

At this point we wish to consider the ^{13}CO behaviour in the southern part of the component B. We have only detected this molecule near the peak of the CO emission. This indicates that this is a *unique* region where the ^{12}CO/^{13}CO changes appreciably, most likely due to an increase of the opacity in the ^{12}CO lines. Only $1'$ to the east of this position (essentially one beam) there is no significant emission in ^{12}CO from the component B, just at the western border of the component A2. This spatial anti-correlation between components A2 and B is also present toward the southern interface. Furthermore, there is a bridge in the CO emission which seems to connect both components within a small area (see slice 3 of Fig. 4), suggesting that both components are related. The CO in the HII region might be heated by the WR radiation field (St-Louis et al. 1998), but the interface between the components A2 and B may not be excited by the same mechanism.

All these observational facts can be explained in a scenario in which a shock of 10–14 km s^{-1}, driven by the expanding hot bubble, impacts on the component A2. As a consequence of the shock, the gas was accelerated up to the velocities of the component B. The large width of the component B when compared with the component A2 can be understood by means of an increase of the turbulent motion due to the energy injected by the shock. Furthermore, the systemic velocity of the HI shell found at larger scales (presumably near the rest velocity of the gas) is also similar to the velocity of the component A2, supporting this scenario. The shock heats the gas and forms a *thin layer* of compressed material with large H_2 density and with high opacity in the ^{12}CO. This thin shocked layer would remain unresolved by the beam. The kinematics shown in Fig. 4 and the low ^{12}CO/^{13}CO ratio at 53–56 km s^{-1} towards the CO peak are very suggestive of this thin shocked layer. Indeed, the large optical depth of the CO lines can only be explained if this emission arises from a very small region unresolved by the beam, probably less than 0.2 pc wide. Furthermore, the large CO column density of $B^{\rm red}_{\rm max}$ as compared with $B^{\rm blue}_{\rm max}$ would indicate large densities for these radial velocities (up to several 10^4 cm^{-3}). Obviously, in the scenario of the shocked gas responsible for the component B, $B^{\rm red}_{\rm max}$ would represent the material which has been recently shocked. High angular resolution observations are needed to disclose this particular region and to check our interpretation.

Although our hypothesis seems reasonable, it should be pointed out that this shocked region is small and it cannot be spatially resolved in our data. Another crucial

point is the weakness of the "bridge" which connects the components A2 and B. Higher angular resolution and more sensitive observations are needed to confirm the presence of the shocked layer and to fully study its properties. If this is the case, NGC 2359 would have the first direct evidence of shocked molecular gas in a WR environment. The O-stage of HD 56925 have created in the ISM the HI shell reported in this paper and the IRAS shell reported by Marston (1996). In consequence, the optical nebula and its surroundings, where we find most of the CO emission, have a more recent origin than the large scale HI shell. The HII region has a size that indicate a dynamical age of less than 10^5 yr. This age is comparable with the WR or a previous phase, such as LBV or RSG (Maeder & Meynet 1994). On the other hand, many optical shells of enriched material are found close to the WR star (Esteban et al. 1990). This leads us to think that the material now interacting with the HII region was ejected in previous episodes of RSG or LBV phase. Chemical studies using other molecular line transitions, especially those capable of tracing the molecular gas enriched by these phases, will definitively confirm or discard these ideas.

5. Conclusions

We have analyzed the large-scale 21 cm-HI emission in a $6° \times 6°$ field around the nebula NGC 2359, and found a large expanding bubble roughly centered at the nebula and its exciting star, the Wolf-Rayet HD 56925. The systemic velocity of the bubble is ∼64 km s^{-1} and it is expanding at 12 km s^{-1}. At an assumed distance of 5 kpc, the bubble has a size of 70×37 pc and a HI mass between 700 and 2400 $M_\odot$. By simple estimates of energetics, ages and stellar wind parameters, we think that this feature is a wind-blown bubble produced by the O-progenitor of the WR star. The presence of a nearly spatially-coincident IRAS shell reinforces our hypothesis.

We have also mapped the CO $J = 1 \rightarrow 0$ and $2 \rightarrow 1$ emission adjacent to NGC 2359 and found three CO components in this region. Two of these components, with radial velocities of 34 (component A1) and 67 (component A2) km s^{-1}, have narrow profiles (up to 2 km s^{-1}) and do not show any morphological or kinematical effects which indicate the disturbance by the nebula or the WR star. However, the third component (the component B, emitting at 54 km s^{-1}), clearly bounds NGC 2359 at its southern and eastern border. The profiles are broad, with linewidths of 4–5.5 km s^{-1}. A velocity gradient of a few km s^{-1} is noted towards the south and south-eastern interface with the nebula. A weak "bridge" in velocity of small angular extension seems to connect this component with the component B2 at the southern part.

We have observed the ^{13}CO $J = 1 \rightarrow 0$ line at a few points in the region where the component B is detected. We have found a striking variation of the ^{12}CO/^{13}CO ratio both in position and in velocity. This ratio seems to decrease near the peak of the CO emission, for velocities higher than 53 km s^{-1}. This particular emiting region is not resolved by the beam, and is probably 0.2 pc wide.

From the observational data, we have estimated the physical conditions for each CO component using the LVG approximation. The highest excitation temperature and density are found in the component B. It is remarkable that high temperatures (up to 80 K) are derived for the CO emission projected onto the HII region.

In view of the kinematics, the morphology and the physical properties of the CO, we think that the component A2 was shocked and accelerated by the expanding bubble to reach the radial velocities of the component B. The shock front is still acting at the southern part of the region. The origin of such shock might be related to the WR phase of HD 56925 or, more probably, to previous episodes of RSG of LBV. From the ^{12}CO/^{13}CO ratio we infer the presence of a thin layer of dense gas which represent the more recently shocked material. Our data, however, cannot resolve spatially the region where a thin layer of shocked material is expected. CO observations with better resolution and sensitivity is needed to disclose the main features of the region.

References

Arnal, E. M. 1992, A&A, 254, 305
Arnal, E. M., & Cappa, C. E. 1996, MNRAS, 279, 788
Arnal, E. M., Cappa, C. E., Rizzo, J. R., & Cichowolski, S. 1999, AJ, 118, 1798
Cappa, C. E., & Benaglia, P. 1998, AJ, 116 1906
Cappa, C. E., Dubner, G. M., Rogers, C., & St-Louis, N. 1996, AJ, 112, 1104
Cappa, C. E., Goss, W. M., Niemela, V. S., & Ostrov, P. G. 1999, AJ, 118, 948
Chu, Y.-H., Treffers, R. R., & Kwitter, K. B. 1999, ApJS, 53, 937
Chu, Y.-H., Weis, K., & Garnett, D. R. 1983, ApJ, 117, 1433
Esteban, C., Vilchez, J. M., Manchado, A., & Edmunds, M. G. 1990, A&A, 227, 515
Dyson, J. E. 1989, IAU Colloq., 120: Structure and Dynamics of the Interstellar Medium, 137
Fich, M., Blitz, L., & Stark, A. A. 1989, ApJ, 342, 272
Fich, M., & Silkey, M. 1991, ApJ, 366, 107
García-Segura, G., & Mac Low, M. 1995, ApJ, 455, 145
Goudis, C. D., Christopoulou, P.-E., Meaburn, J., & Dyson, J. E. 1994, A&A, 285, 631
Goudis, C., Hippelein, H., & Münch, G. 1983, A&A, 117, 127
Hartmann, D., & Burton, W. B. 1997, Atlas of galactic neutral hydrogen (Cambridge, New York: Cambridge University Press)
Kutner, M. L., & Ulich, B. L. 1981, ApJ, 250, 341
Langer, N., Hamann, W.-R., Lennon, M., et al. 1994, A&A, 290, 819
Lockman, F. J. 1989, ApJS, 71, 469
Maeder, A., & Meynet, A. 1994, A&A, 287, 803
Marston, A. P. 1991, ApJ, 366, 181
Marston, A. P. 1996, AJ, 112, 2828
Marston, A. P., Welzmiller, J., Brandsford, M. A., Black, J. H., & Bergman, P. 1999, ApJ, 518, 769
McCray, R. 1983, Highlights Astron., 6, 565

Moffat, A. F. J., Marchenko, S. V., Seggewiss, W., et al. 1998, A&A, 331, 949
Rizzo, J. R., & Arnal, E. M. 1998, A&A, 332, 1025
Rizzo, J. R., & Bajaja, E. 1994, A&A, 289, 922
Rochowicz, K., & Niedzielski, A. 1995, Acta Astron., 45, 307
St-Louis, N., Doyon, R., Changnon, F., & Nadeau, D. 1998, AJ, 115, 2475
Schneps, M. H., Haschick, A. D., Wright, E. L., & Barret, A. H. 1981, ApJ, 243, 184
Van Buren, D. 1986, ApJ, 306, 538
van der Hucht, K. A. 2000, New Astron. Rev., in press
Weaver, R., McCray, R., Castor, J., Shapiro, P., & Moore, R. 1977, ApJ, 218, 377
Wilson, T. L., & Matteucci, F. 1992, A&AR, 4, 1